## Supplementary Material

### Detailed methodology

*Monitoring of anesthetic agents in serum samples*

Propofol was detected in serum samples using HPLC (Waters 1525 Binary HPLC Pump and Waters 2489 UV/ Visible Detector). Samples were separated in HPLC with a reversed-phase NOVA PAK C18 column (2.1 mm × 150 mm, 3 µm; Thermo Fisher Scientific, Waltham, MA, USA) at a wavelength of 270 nm. The mobile phase was a mixture of water-acetonitrile (40:60 v/v) with a flow rate of 1ml/ min was pumped isocratically through the column. Spiked serum samples with propofol (1000 µg/ml; Fig. 1A) were detected at a retention time of 3.023 min. The tubes containing 100 µl of serum samples mixed with 100 µl of acetonitrile were vortex mixed for 10 s and centrifuged at 2000 × g for 15 min. The supernatant was then removed to a clean glass test tube. The samples were maintained at room temperature and the injection volume was 20 µl. Propofol was detected only in the intraoperative period at a retention time of 3.032 min (Supplementary Fig. 1C). However, at a retention time of 3.032 min, nothing was detected in the pre and postoperative serum samples (Supplementary Fig. 1B and D).

Fluoride concentration during the pre, intra and postoperative periods after isoflurane anesthesia were measured from serum samples using Fluoride Ion Selective Electrode technique (Thermo Scientific Orion Star A214 Ph/ISE Benchtop Meter). We found that the soluble serum fluoride concentration was increased in the intraoperative serum compared to pre and postoperative samples (Supplementary Fig. 1E).

*Flow cytometry for detection of lymphocyte subtypes*

The immunophenotype of the lymphocytes was analyzed with flow cytometry. Whole blood (100 µl) was added with a cocktail of fluorescent-tagged antibodies [{anti-human CD3 (UCHT1), allophycocyanin (APC)-Cyanine7;

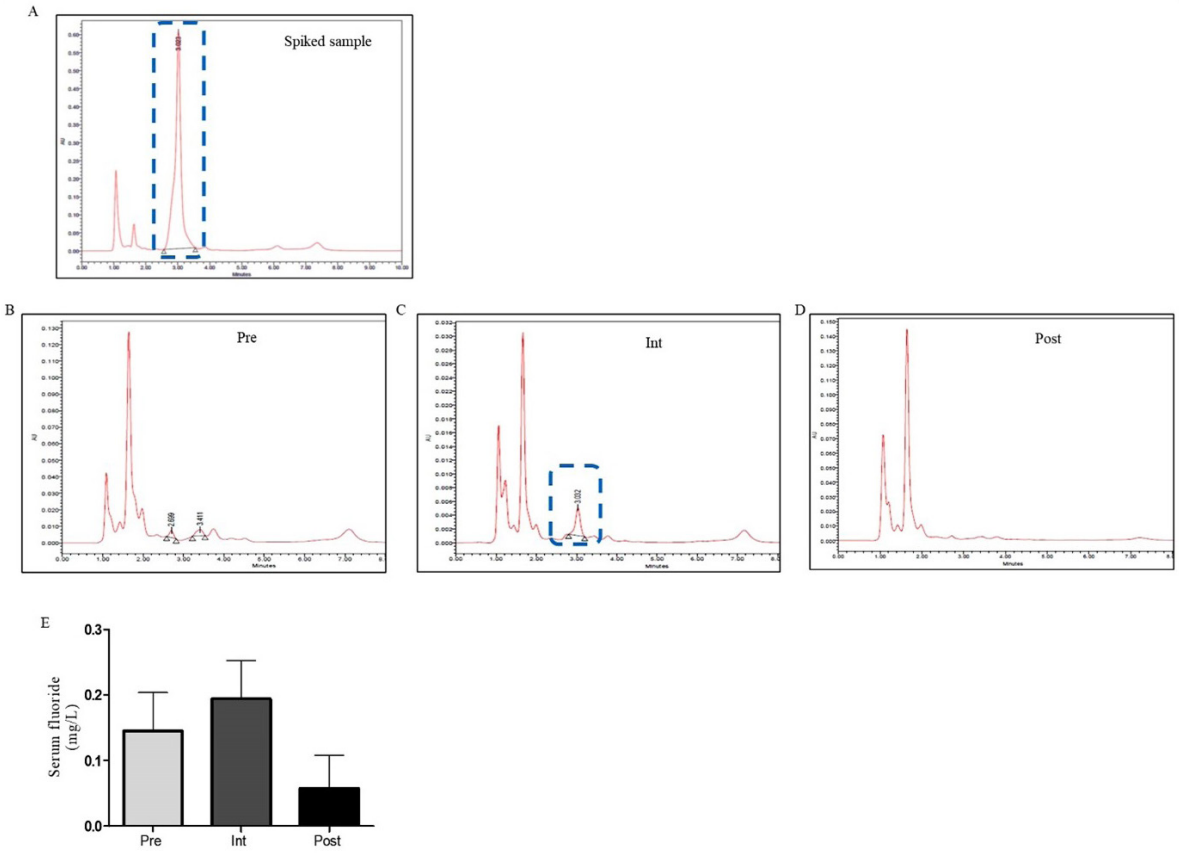


**Supplementary Fig. 1**. Chromatograms of propofol from pre, intra and postoperative serum samples. (**A**) Chromatogram of propofol from the serum sample spiked with 1000 µg/ml propofol; (**B**) chromatograms of propofol from the preoperative; (**C**) intraoperative; (**D**) postoperative serum samples of representative patient anesthetized with propofol; (**E**) concentration of serum fluoride (mg/l) in pre, intra and post samples. Pre, preoperative; Int; intraoperative; Post, postoperative.

anti-human CD19, fluorescein isothiocyanate (FITC); anti-human CD4 (S3.5), PE-Texas Red; anti-human CD8, FITC; anti-human CD28 (CD28.2), PerCP-Cyanine5.5 and anti-human T cell receptor (TCR) (IP26), alexa fluor (AF) 700} Invitrogen, Thermo Fisher Scientific Waltham, MA, USA] diluted in phosphate buffer saline (PBS), and was incubated in dark for 45 min, at 4°C. Thereafter the erythrocytes were lysed with FACS™ lysing solution 1× concentrate [BD Biosciences, San Jose, CA, USA] washed with ice-cold PBS, resuspended in paraformaldehyde (2%), kept at 4°C and analyzed within 24 h using flow cytometer [BD LSRFortessa cell analyzer, Franklin Lakes, NJ, USA] and the software BD FacsDiva 9.0.1. Data were analyzed in FlowJo version 10.8.1 [BD, Franklin Lakes, NJ, USA].

*Gating strategy for T cells*: For data analysis, the following population were gated sequentially. At first, the white blood cells were gated for lymphocytes by forward vs side scatter (FSC: SSC) plot (Supplementary Fig. 2A) and further the gated lymphocytes were checked for singlets in another FSC-height (H) vs FSC area (A) plot (Supplementary Fig. 2B). Next the lineage marker CD3 was gated as CD3+ population or CD3- population [based on unstained negative control] in an SSC vs CD3 plot (Supplementary Fig. 2C). CD3+ population was further gated for CD4 and CD8 subsets in CD8 Vs CD4 plot (Supplementary Fig. 2D). CD4+CD8- population was subsequently analyzed for TCR+ cells in CD4 vs TCR quadrant plot (Supplementary Fig. 2E) and for CD28+ cells in a CD4 vs CD28 quadrant plot (Supplementary Fig. 2F). Similarly, CD4-CD8+ population was analyzed for TCR+ cells (Supplementary Fig. 2G) and CD28+ cells (Supplementary Fig. 2H). Compensation was done with single stained samples. Compensation was further corrected with each patient, if needed. The same gate was applied for pre-, intra- and postoperative blood samples of each patient to maintain the uniformity of gating strategy.

*Gating strategy of B cells*: For data analysis, the following population were gated sequentially. At first, the white blood cells were gated for lymphocytes by forward vs side scatter (FSC: SSC) plot (Supplementary Fig. 3A) and further the gated lymphocytes were checked for singlets in another FSC-H vs FSC-A plot (Supplementary Fig. 3B). Next the lineage marker CD3 was gated as CD3+ or CD3- populations [based on unstained negative control] in an SSC vs CD3 plot (Supplementary Fig. 3C). Subsequently CD3- cells were analyzed for CD19+ B cells in a quadrant

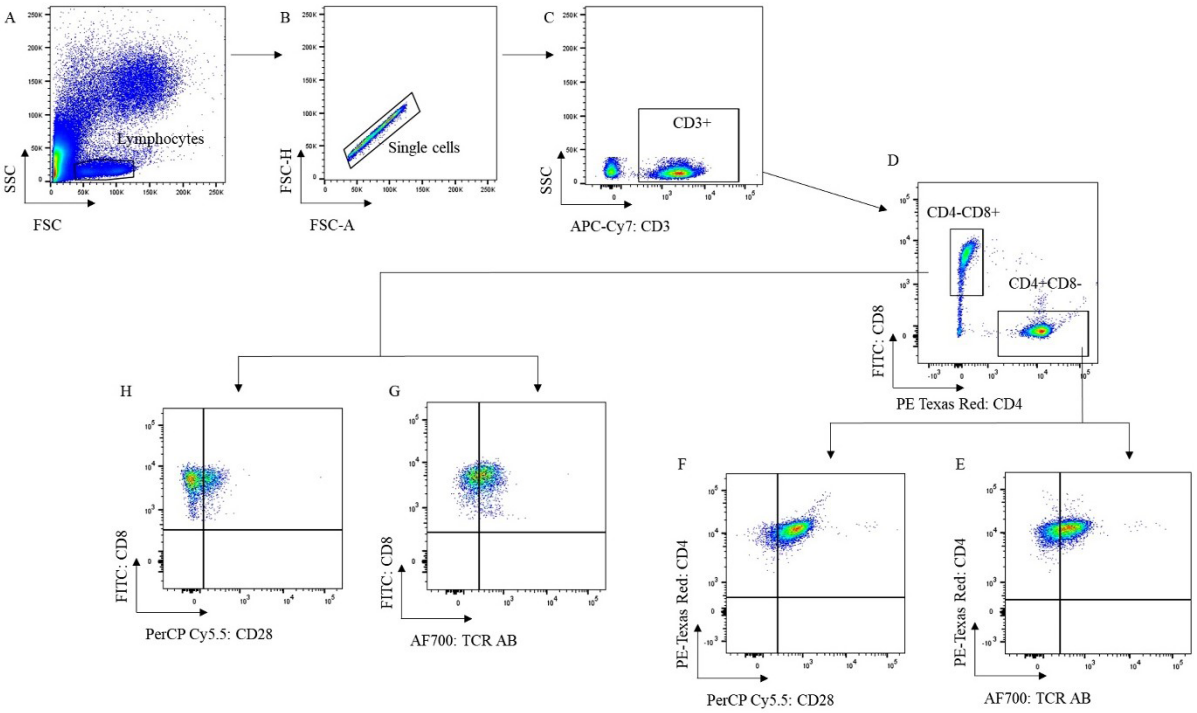


**Supplementary Fig. 2**. Gating strategy of T cells. (**A**) Gating of lymphocytes; (**B**) single cells of lymphocyte population; (**C**) CD3+ lymphocyte population; (**D**) CD3+CD4+CD8- and CD3+CD4-CD8+ T cells; (**E**) CD3+CD4+CD8-TCR+ T cells; (**F**) CD3+CD4+CD8-CD28+ T cells; (**G**) CD3+CD4-CD8+TCR+ T cells; (**H**) CD3+CD4-CD8+CD28+ T cells.

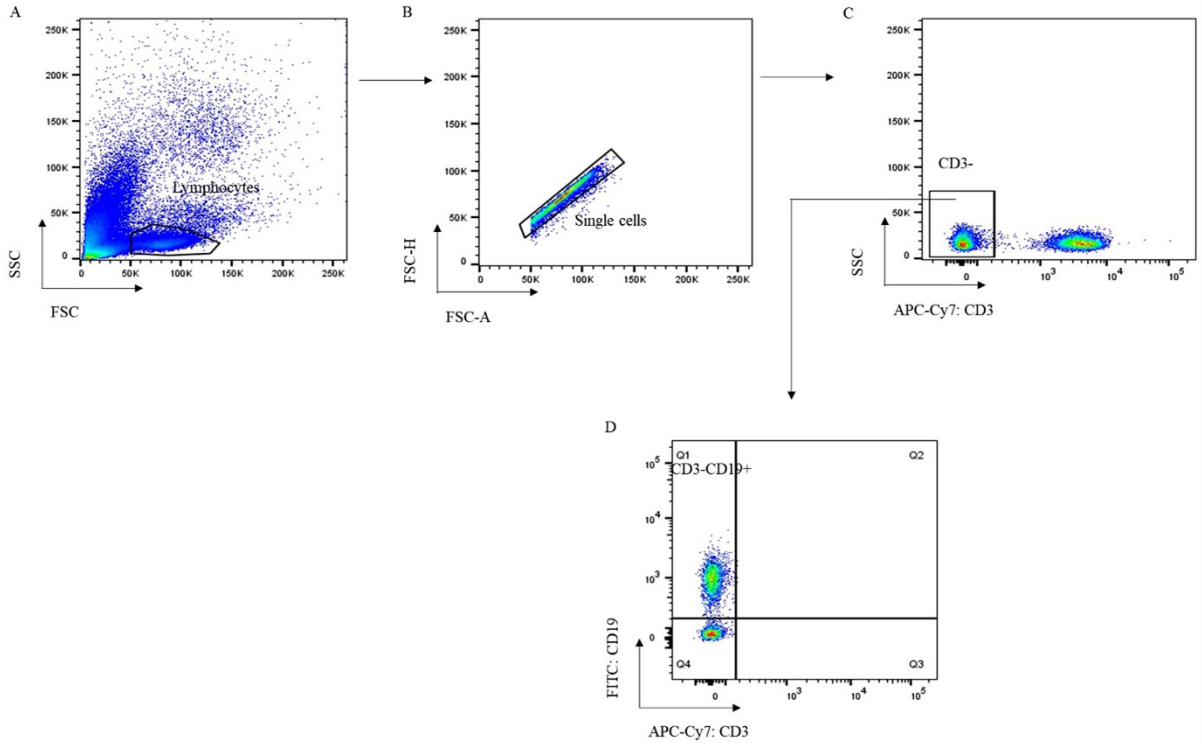


**Supplementary Fig. 3**. Gating strategy of B cells. (**A**) Gating of lymphocytes; (**B**) single cells of lymphocyte population; (**C**) CD3- lymphocyte population; (**D**) CD3-CD19+ B cells.

plot (Supplementary Fig. 3D). Compensation was done with single stained samples. Compensation was further corrected if needed with different populations. The same gate was applied for pre, intra and postoperative blood samples of each patient to maintain the uniformity of gating strategy and to obtain the corresponding statistics.

*Effect of isoflurane/propofol on T cell activity markers*: The decrement of Th and Tc cell frequency within the isoflurane group prompted us to check the effect of isoflurane/propofol on the TCR and CD28 activity. TCRs are involved in the recognition of ligands bound to major histocompatibility complex presented on antigen-presenting cells. We did not observe any significant difference of CD4+TCR (Supplementary Fig. 4A, C) and CD8+TCR (Supplementary Fig. 4B, C) between the time points within the isoflurane/propofol groups. CD28, a major costimulatory molecule required for full activation of T cells, is expressed in 95% of the resting CD4+T cells and 50% of the resting CD8+T cells in human peripheral blood. Similar to TCR, CD28 too did not show any significant difference in the activity of CD4 (Supplementary Fig. 4D, F) and CD8 cells (Supplementary Fig. 4E, F) between the anesthetic groups of isoflurane/propofol.

## *In silico* analysis

*Sequence, structure, and functional analysis*

The sequence, structure, and functional information of CD4 and CD8 were retrieved from the UniProtKB database with ID P01730 (CD4_HUMAN) and P01732 (CD8A_HUMAN) respectively. The X-Ray diffraction structures of CD4 (PDB ID- 1WIO) and CD8 (PDB ID- 1CD8) with resolution 3.90 Å/amino acid (aa) length 363 and 2.60 Å/ aa length 114 respectively were retrieved from PDB database. The co-crystallized compounds/macromolecules/water molecules were removed using BIOVIA Discovery Studio 4.5 Visualizer (BIOVIA, San Diego, CA, USA).

*Prediction of binding site*

The binding region of CD4 and CD8 were predicted using the consensus outcomes of the Computed Atlas of Surface Topography of Proteins, Grid-based Hemi pocket finder at (*https://pdbj.org/ghecom/*) and DEPTH (*http://*

**Supplementary Table I.** Type III Tests of Fixed Effects with Th as dependent variable

| Source | Numerator df | Denominator df | F | *P* value |
|---|---|---|---|---|
| Intercept | 1 | 58.000 | 1.734 | 0.193 |
| Timepoints | 2 | 196.000 | 1.186 | 0.308 |
| Arm | 1 | 58.000 | .950 | 0.334 |
| Arm with timepoints | 2 | 196.000 | 8.323 | 0.000 |
| Type of surgery | 1 | 58.000 | 1.267 | 0.265 |
| Arm with type of surgery | 1 | 58.000 | .992 | 0.323 |
| Histopathology | 3 | 58.000 | .641 | 0.592 |
| Arm with histopathology | 3 | 58.000 | .446 | 0.721 |
| Stage | 2 | 58 | .511 | 0.603 |
| Arm with stage | 2 | 58 | .241 | 0.787 |
| Molecular subtypes | 5 | 58 | 1.244 | 0.301 |
| Arm with molecular subtypes | 5 | 58 | .117 | 0.988 |
| ASA | 1 | 58 | 1.942 | 0.169 |
| Arm with ASA | 1 | 58 | .300 | 0.586 |
| Grade | 2 | 58 | .405 | 0.669 |
| Arm with grade | 2 | 58 | 1.467 | 0.239 |
| Age | 1 | 58.000 | 4.338 | 0.042 |
| Arm with age | 1 | 58.000 | 1.093 | 0.300 |
| Height | 1 | 58.000 | .628 | 0.431 |
| Arm with height | 1 | 58.000 | .564 | 0.456 |
| Weight | 1 | 58.000 | 1.449 | 0.234 |
| Arm with weight | 1 | 58.000 | 2.431 | 0.124 |
| Duration_anesthesia | 1 | 58.000 | .794 | 0.377 |
| Arm with duration_anesthesia | 1 | 58.000 | 2.170 | 0.146 |
| Duration_surgery | 1 | 58.000 | 1.351 | 0.250 |
| Arm with duration_surgery | 1 | 58.000 | .891 | 0.349 |
| Pain_score | 1 | 58 | 1.098 | 0.299 |
| Arm with pain_score | 1 | 58 | .231 | 0.633 |

df, degrees of freedom; F, Fisher's test

*cospi.iiserpune.ac.in/depth*) and all the coordinates like x y z was set by using the AutoDock 4.2 software *(https://autodock.scripps.edu/download-autodock4/)*.

*Retrieval of drugs*

The structural information of isoflurane and propofol was obtained from PubChem with Compound IDs: 3763 and 4943 in Structure Data Format. The structures were converted to .pdb format, which is mostly preferred format for different docking tools.

*Molecular docking studies*

GLIDE (Grid-based Ligand Docking with Energetics, Schrödinger Release 2021-1: Maestro, Schrödinger, LLC, New York, NY, 2021) was used for docking analysis of isoflurane and propofol against CD4 and CD8 targeted proteins in extra precision mode. The best docked complexes were characterized and processed for further computational analysis based on binding energy values, intermolecular hydrogen (H)-bonds, as well as other

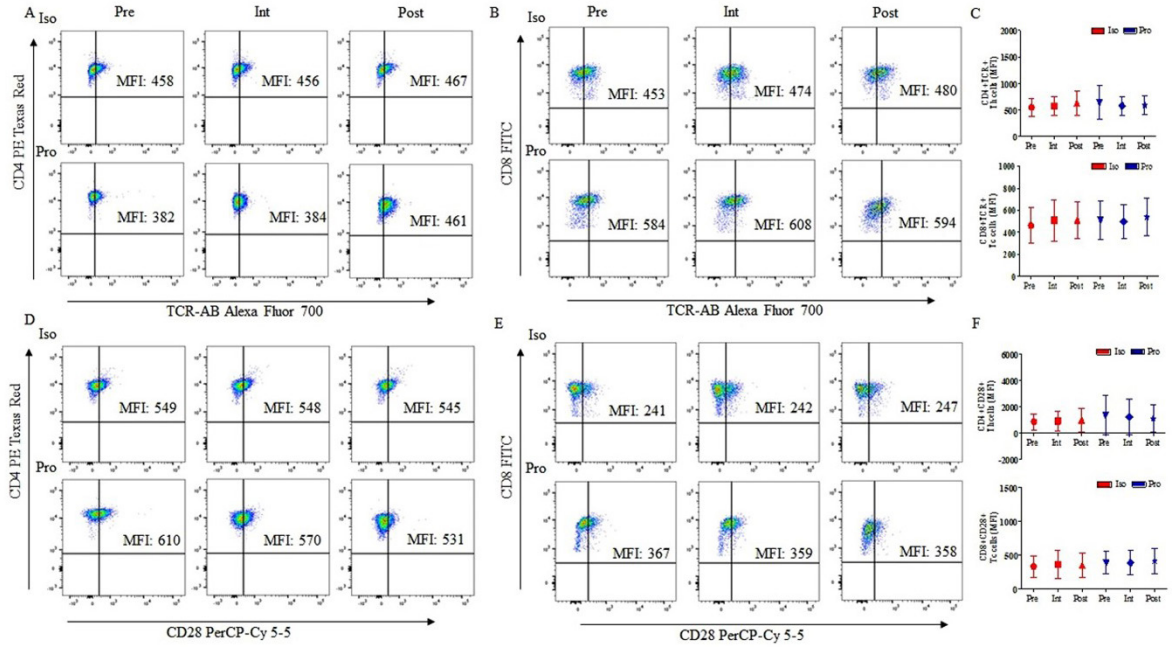


**Supplementary Fig. 4.** Flowcytometric analysis of TCR and CD28 expression in CD4 and CD8 T cells in peripheral blood of breast cancer patients at pre-, intra-, and postoperative periods of Iso and Pro groups. The (**A**) CD4+TCR, (**B**) CD8+TCR, (**D**) CD4+CD28, and (**E**) CD8+CD28+ cells in representative female anesthetized with Iso/Pro; comparative effect of Iso and Pro on (**C**) CD4+TCR+ and CD8+TCR+ cells; (**F**) CD4+CD28+ and CD8+CD28+ cells at different time points among breast cancer patients. Data represented as mean fluorescent intensity (MFI) and the graphs were plotted based on the mean±SD. Iso, isoflurane; Pro, propofol; Pre, preoperative; Int, intraoperative; Post, postoperative.

hydrophobic and electrostatic interactions. LigPlot+ (*https://www.ebi.ac.uk/thornton-srv/software/LigPlus/*) and the ligand interactions module of Schrödinger were used to show the presence of intermolecular bonds between protein-drug complexes. Apart from Glide, docking of propofol and isoflurane against CD4 and CD8 was also rechecked using Autodock4.2 docking tool.

*Molecular dynamics (MD) simulations*

Desmond programme was used for MD simulations of the Holo-1: CD4-isoflurane complex, Holo-2: CD4-propofol complex, Holo-3: CD8-isoflurane complex, and Holo-4: CD8-propofol complex, to understand the dynamic behaviour, mode of binding and inhibitor specificity for all the systems. The targeted protein and protein–ligand/drug complex structures were considered from the final docked structures. A 100 nano second (ns) MD simulation was used to assess receptor structural rearrangements as well as the stability of the docked complexes with isoflurane and propofol. MD protocol followed minimization, heating, equilibration, and production. The OPLS4 force field was used to minimize the protein-ligand complexes, and topology, and thus atomic coordinates were obtained automatically. Subsequently, the compound was immersed in an SPC solvent model orthorhombic box (15×15×10 Å). By adding 0.15 M NaCl, the physiological pH was neutralized. Using the Particle Mesh Ewald (PME) boundary condition, the water box was configured to ensure that no solute atoms occurred within a 10 Å distance of the border. The entire system was simulated at 300 K for 100 ns using the NPT ensemble, and the structural alterations and dynamic behaviour of the proteins were investigated using root mean square deviation (RMSD) and root mean square fluctuation (RMSF) graphs. The difference between the backbones of a protein from its initial structural conformation to its ultimate position was measured using RMSD. The RMSF method was used to find the flexible region of a protein or complex. The simulation interaction diagram depicted the most likely ligand binding mode at the protein's binding site.

*Annotation of binding/active site of CD4 and CD8*: The consensus results of CASTp, GHECOM, and DEPTH web server depicted the residues His 132, Leu 133, Leu 134, Leu 176, Ser 179, Val 200, Val 201, Leu 202,203ala, Phe

204, Phe 223, Pro 224, Leu 225, Ala 226, Phe 227, Thr 228, Val 229, Glu 230, Thr 233, Gly 234, Ser235, Leu256, Lys257, Asn258, Lys259, Leu278, Pro 279, Leu 280, Leu 299, Ala 300, Leu 301, Glu 302, Lys 304 for CD4 and Ser52, Gly53, Ser55, Leu57, Phe69, Tyr72, Ser116, Ala117, Leu118, Met123, Phe125 for CD8 targeted protein that takes part in active site formation.

*H-bond analysis*: During MD simulations, the intermolecular hydrogen bonds of the Holo states were plotted using Schrödinger Release 2021-1 (Supplementary Fig. 5). Simulation of all the Holo states revealed variation of intermolecular hydrogen bonds during the simulation. The post-MD simulation analysis revealed one conventional H-bond in Holo-2, and Holo-4 was retained whereas none were observed in Holo-1 and Holo-3 (Supplementary Fig. 5). The number of H-bonds was directly proportional to the stability of the drug-target complex during the complete simulation period. The stacked bar chart of Holo-1 in Supplementary Fig. 5A illustrated that amino acid residues of CD4 such as Ala226, Thr228, and Glu348 played a key role in the protein's binding, regulation, and activity. Some protein residues may make several interactions of the same subtype with the ligand, and values above 0.00075 were indicative of such plausible interactions in this histogram. Holo-1 represented a consistent number of intermolecular hydrogen bonds throughout the simulation (Supplementary Fig. 5A). No H-bond interactions were represented during post-MD of Holo-1 (Supplementary Fig. 5A). While simulations of Holo-1, H-bond forming residue such as Thr228 was broken down but later it was compensated by novel hydrophobic interactions, and van der Waals interactions **(**Supplementary Fig. 5A).

The stacked bar chart of Holo-2 (Supplementary Fig. 5B) depicted that amino acid residues of CD4 such as Ala226, Thr228, and Glu230 mediated a major role in the binding and regulation of the protein. Values of protein residues above 0.4 were indicative of multiple interactions of the same subtype with the ligand. Holo-2 state represented a consistent number of intermolecular hydrogen bonds throughout the simulation (Supplementary Fig. 5B). One H-bond (Thr228) was represented in the case of post-MD of Holo-2. While simulations of Holo-2, H-bond forming residue such as Thr233, which was broken, was compensated with few novel hydrophobic interactions, and van der Waals interactions **(**Supplementary Fig. 5B).

Similarly, in the case of CD8 protein (Holo-3 and Holo-4), the stacked bar chart of Holo-3 (Supplementary Fig. 5C) showed that amino acid residues such as Gln75, and Ser116, controlled the binding and regulation of the protein. The values of 0.002 of protein residues indicated multiple interactions of the same subtype with the ligand. Holo-3 state represented a consistent number of intermolecular hydrogen bonds throughout the simulation (Supplementary Fig. 5C). No H-bond was represented in the case of post-MD of Holo-3. During simulations of Holo-3, H-bond forming residue such as Ser55 was broken down but later it was compensated with novel hydrophobic interactions, and van der Waals interactions (Supplementary Fig. 5C). Holo-4, stacked bar chart (Supplementary Fig. 5D) exhibited that the amino acid residues Ser55, Ala64, maneuvered the binding and regulation of the protein. Protein residues with values above 0.10 indicated several interactions of the same subtype with the ligand. Holo-4 state represented a consistent number of intermolecular hydrogen bonds throughout the simulation (Supplementary Fig. 5D). One H-bond was represented in the case of post-MD of Holo-4. During simulations of Holo-4, H-bond forming residue such Ser116 did not break but a few novel hydrophobic interactions and van der Waals interactions were compensated (Supplementary Fig. 5D). Ser116 did not get compensated which indicated that it might have been a crucial residue in restricting suppression of CD8 by propofol.

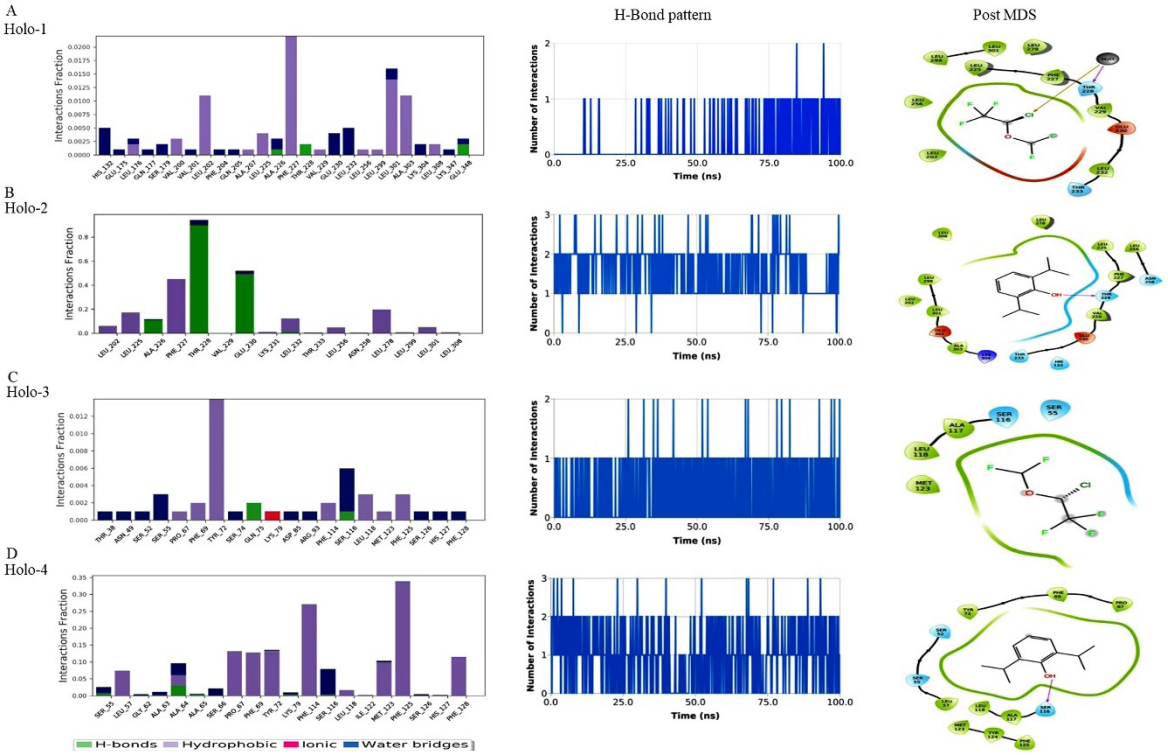


**Supplementary Fig. 5.** Hydrogen bond analysis of isoflurane and Propofol with CD4 and CD8. Stacked bar chart showing protein-ligand contacts plot, deviation of H-bonds contributing to interaction during 100 ns simulation and post-MD simulations intermolecular hydrogen bonding, electrostatic and hydrophobic contacts formed between (**A**) Holo-1; (**B**) Holo-2; (**C**) Holo-3; (**D**) Holo-4 complex. Holo-1, CD4-isoflurane complex; Holo-2, CD4-propofol complex; Holo-3, CD8-isoflurane complex, and Holo-4:CD8- propofol complex.